JMEPEG (2017) 26:3079–3089
DOI: 10.1007/s11665-017-2734-3

1059-9495/$19.00

A Comparative Study of Thermal Conductivity and Tribological Behavior of Squeeze Cast A359/AlN and A359/SiC Composites

Essam. A.M. Shalaby, Alexander. Yu. Churyumov, Dina. H.A. Besisa, A. Daoud, and M.T. Abou El-khair

(Submitted October 31, 2016; in revised form April 17, 2017; published online May 24, 2017)

A comparative study of thermal and wear behavior of squeeze cast A359 alloy and composites containing 5, 10 and 15 wt.% AlN and SiC particulates was investigated. It was pointed out that A359/AlN composites have a superior thermal conductivity as compared to A359 alloy or even to A359/SiC composites. Composites wear characteristics were achieved by pins-on-disk instrument over a load range of 20-60 N and a sliding speed of 2.75 m/s. Results showed that A359/AlN and A359/SiC composites exhibited higher wear resistance values compared to A359 alloy. Moreover, A359/AlN composites showed superior values of wear resistance than A359/SiC composites at relatively high loads. Friction coefficients and contact surface temperature for A359/AlN specimens decreased as AlN content increased, while they increased for A359/SiC. Investigations of worn surfaces revealed that A359/AlN composites were covered up by aluminum nitrides and iron oxides, which acted as smooth layers. However, A359/SiC composites were mainly covered only by iron oxides. The superior thermal conductivity and the significant wear resistance of the developed A359/AlN composites provided a high durable material suitable for industrial applications.

Keywords friction coefficient, metal-matrix composite, squeeze, thermal conductivity, wear

1. Introduction

Using lightweight and durable materials for automotive and aerospace industries is one of the highest increased requirements of the global market for saving energy and for keeping green environment via reducing fuel consumption. Potential attentions have been directed to aluminum metal-matrix composites (AMMCs) due to their significant mechanical, tribological and thermal characteristics versus conventional aluminum alloys. Thus, their wonderful properties have nominated them for aerospace and automotive industries (Ref 1-10). In dry wear, ductile materials as aluminum alloys usually exhibit severe wear (Ref 11-18). On the other hand, in recent years, various kinds of reinforcements have been applied to develop and enhance the performance of AMMCs in industry (Ref 19-28). This can be ascribed to the superior appealing properties over the traditional aluminum alloys. For example, a reduction in the wear rate of Al-Si alloy accompanied by the addition of 15 to 20 with % SiC was noted by Pramila et al. (Ref 29).

Essam. A.M. Shalaby and **Alexander. Yu. Churyumov**, National University of Science and Technology (NUST) "Moscow Institute of Steel and Alloys (MISiS)", Leninskiy st. 4, Moscow 119049, Russian Federation; **Dina. H.A. Besisa**, National University of Science and Technology (NUST) "Moscow Institute of Steel and Alloys (MISiS)", Leninskiy st. 4, Moscow 119049, Russian Federation; and Central Metallurgical Research and Development Institute "CMRDI", P.O. Box 87, Helwan, Egypt; and **A. Daoud** and **M.T. Abou El-khair**, Central Metallurgical Research and Development Institute "CMRDI", P.O. Box 87, Helwan, Egypt. Contact e-mail: essam@misis.ru.

SiC ceramic particulates have been long used successfully and extensively as reinforcement for A359 matrix alloy. They own appealing high temperature, electrical and thermal properties. They have high hardness, strength, Young's modulus, significant wear and corrosion resistance, low thermal expansion coefficient and low cost (Ref 19, 30-33). Several works have considered the effect of SiC addition on the properties of A359 alloy. Shalaby et al. (Ref 34) discussed the influence of (SiC + Si_3N_4) addition on the microstructure and mechanical properties of A359 composites. They produced successfully lightweight hybrid composites with high mechanical properties and high potential use in automotive and aerospace applications. Daoud et al. (Ref 19) reported a significant enhancement in dry wear of A359-Si/20 vol.% SiC particulates. They have added 20 vol.% SiC to A359 composites in an attempt to upgrade the alloy wear resistance. At load of 50 N and speed range of 3-12 m/s, the worn surface of the composite disk showed a dark adherent layer, which mostly consisted of the constituents of the friction material. This layer acted as a protective coating and lubricant, resulting in an improvement in the wear resistance and friction coefficient of the A359 composite. Moreover, Przestacki et al. (Ref 35) have studied the improvement of surface quality and wear resistance of A359 composite through 20% SiC addition during laser-assisted turning. Further work of Rohatgi et al. (Ref 36) has examined the effect of foundry, composite ingot supplier, testing laboratory, volume (%) SiC, mold type and surface finish (machining or non-machining), on the tensile properties of cast SiC-reinforced Al-matrix composites. Neutron diffraction method was used to study and analyze the creep and damage occurrence in an A359/SiC composite (Ref 37). Another interesting work concerning A359/SiC composite was accomplished by Rodríguez-Castro et al. (Ref 38). They have investigated the microstructure and mechanical properties of functionally graded A359/SiC composite produced by centrifugal casting. The produced composite has a uniform and gradual distribution of SiC reinforcements in the alloy as well as a high tensile strength. Many investigations discussed the

influence of SiC reinforcements on the performance and properties of A359 alloy (Ref 39-41).

On the other hand, AlN ceramic has superior hardness, strength, wear resistance, thermal and electrical conductivity. Besides, it has a low density and coefficient of thermal expansion. Its superior thermal and mechanical characteristics nominate it to become an important competitive candidate in the industry. For example, it can be utilized in pistons, brake rotors and brake drums in automotive industries where heat sink and significant wear resistance are required. Also, it can be used in aerospace structures as semiconductor packaging. Regarding to its potential thermal properties, it also has been applied for refractory applications. Despite the great importance of AlN ceramics, there are only few works that have studied the effect of their addition on Al-Si alloys. Gajewska et al. (Ref 42) have investigated the microstructure and properties of 7475 aluminum alloy matrix composites with additions of 10 wt.% of AlN powders with different particle size. It was found that Al alloy matrix composite gave higher strength when reinforced with the micro- rather than with submicro-particles. It suggests that the size of the ceramic phase addition can be considered as only one of the factors influencing the composite strength. Fogagnolo et al. (Ref 43) have inspected the processing, mechanical strength and hardness of aluminum 6061 matrix composite powders reinforced with AlN. Hardness and ultimate tensile strength were extremely increased as compared to that of conventional mixed composites. Moreover, the production, wetting behavior, mechanical properties and microstructure of AMMCs reinforced with AlN ceramic particulates have been investigated. Briefly, AMMCs/AlN composites are promising materials for electronic and thermal sink uses (Ref 21, 25, 44).

Generally, the most frequently used processing techniques of AMMCs are solid- or liquid-state fabrication techniques (Ref 45, 46). Due to the inherent advantages of the liquid-state processing technique, most of commercially AMMCs applications are manufactured by that method. Furthermore, liquid-state process is less expensive, easier to handle than powders and can produce composites in various shapes (Ref 47). Otherwise, stirring technology is common in the AMMCs production (Ref 48). Usually, composites manufactured by stirring technology exhibit a higher porosity percent in comparison with that produced by squeeze casting (Ref 48). Squeeze casting combines the advantages of high pressure application during solidification, permanent mold and forging technology. The squeeze pressure application is directed to develop wear and mechanical properties. It enhances the interfacial strength between the matrix alloy and ceramic reinforcements through eliminating the porosity at the interface, providing better mechanical interlock (Ref 49).

In the present work, the influence of AlN reinforcement addition with different percentages to the A359 matrix alloy was discussed for the first time. SiC particles are also introduced into A359 matrix alloy using the squeeze casting process. The effect of their additions on the thermal conductivity, wear and friction behavior under different loads of the prepared composites was studied. Moreover, a comparative study was established and discussed.

2. Experimental Procedure

2.1 Composites Processing and Thermal Conductivity

In this investigation, A359 alloy was used as the matrix alloy. A359 alloy has a chemical composition (wt.%) of: Si: 9.1%, Mg: 0.58% and rest Al. Aluminum nitride (AlN) and silicon carbide (SiC) are used as two different ceramic reinforcements with a particle size of (40-45)μm. 5, 10 and 15 weight percentages (wt.%) of AlN and SiC were added into A359 matrix. First, composites developed by stirring process. Then, squeeze technique was involved. A359 alloy was melted at 750°C, and skimming was applied to eliminate the impurities from the melt surface before addition of the reinforcements. The melt was rotated gradually by increasing the speed of a titanium stirrer to 850 r.p.m to create the necessary vortex for addition of particulates. The stirring was maintained for 1 min after the addition of the particulates to guarantee a homogeneous distribution of the reinforcements in the matrix. Then, molten composites were immediately poured at a pouring temperature of 680 °C into a pre-heated (200 °C) cylindrical steel mold with an inside diameter of 50 mm. The die and punch temperature was set at 200 °C, while the squeeze pressure was 100 MPa. The holding time during melt pressurization was set to be 1 min. Finally, the solidified samples were ejected.

Squeeze cast A359 composites are used for preparing cylindrical disks of 12.7 mm diameter and 2 mm thickness. Thermal diffusivities of the disk-shaped specimens were evaluated by a NETZSCH-LFA 447 nano-flash thermal analyzer. For each composite type, mean value of four samples was considered. The specific heats of A359 composites were estimated by Setaram Labsys differential scanning calorimetry instrument under the protection of Ar gas. Density of A359 composites was determined by Archimedes' method. The following equation helps to estimate thermal conductivity of various composites: $\lambda = Cp\rho\alpha$, where λ is the thermal conductivity; c_p is the specific heat; α is the thermal diffusivity; and ρ is density.

2.2 Wear

Wear test was achieved using a pin-on-disk apparatus. Pins of 8 mm diameter and 11 mm height were allowed to slide against a rotating steel disk of 200 mm diameter, 3 mm thickness and hardness of 62 HRc. A surface roughness tester Surftest SJ-201P was used to measure the surface roughness (Ra) of the test specimens and steel disk. Ra value of the test specimens and steel disk before the test was 1.45 and 0.35 μm, respectively. The track radius was kept constant at 42 mm, and the disk rotating speed was maintained at 655 r.p.m, resulting in a constant sliding speed of 2.75 m/s. The applied test loads were increased from 20 to 60 N, corresponding to stress levels of 0.40 and 1.19 MPa, respectively. The sliding tests continued without interruption for 30 min. The initial temperature was 20 °C at the beginning of the tests. Within few minutes, the track was smeared with dark debris. No effort was made to clean it. Subsurface temperature was measured using a chromel-alumel thermocouple. The thermocouple was placed in 2-mm-deep holes that drilled in the side surface of the composite specimens at distance 2 mm from the sliding surface. Pin subsurface temperature and friction force were recorded every 5 min. The temperature was recorded to an accuracy of 0.1 °C and the friction force to an accuracy of 0.1 N. From the former data, friction coefficient values were detected. An electronic balance with 0.0001 g sensitivity measured the weight loss of the pin specimens. The wear rate of the pin[R (mm^3/m)] was calculated with the help of the formula (Ref 20): $R = \Delta W/(d \times \rho)$, where ΔW is weight loss,

d is the sliding distance and ρ is the density. After the test, worn surfaces of the pins were examined using scanning electron microscope (SEM) on a microscope Tescan Vega 3 LMH. Moreover, energy-dispersive detector x-ray-Max 80 analysis (EDXA) determined morphology and chemical composition of wear debris.

3. Results and Discussion

3.1 Microstructure and Thermal Conductivity

The microstructure investigation of the squeeze cast composites is illustrated in Fig. 1. The influence of squeeze casting process is clearly announced, where the microstructures are characterized by a relatively uniform distribution of the particles in the A359 matrix alloy. Moreover, there are almost no casting defects. Another important advantage of using a squeeze process is to enhance the wettability between the matrix and the particles at the interface as shown in Fig. 2. It can subsequently result in a good bonding between the composite constituents. Therefore, the mechanical properties are improved (Ref 50). Figure 2(c) shows that the SiC particles are surrounded by A359 matrix after squeeze casting process.

The changes of thermal conductivity of A359/AlN and A395/SiC composites with particulate content are represented in Fig. 3. As revealed, thermal conductivity of A359/AlN slightly increased in a linear manner from 158.2 W/mK to 163.3 W/mK with increasing wt.% of AlN up to 15%. While for A359/SiC composites, it significantly decreased as wt.% of SiC decreased. The main reason is the exceptional thermal conductivity of AlN particulates as compared to that of SiC particulates. However, type of reinforcement is not the only parameter that affects values of thermal conductivity. Particulates grade, weight percentage, bulk densities or porosities percentage and processing technique used are crucial factors which influence the values of thermal conductivity (Ref 24).

Additionally, squeeze technique has a substantial effect on the thermal conductivity of A359/AlN composites. The high pressure used during composite processing guarantees sound composites with low porosity and high bulk density values. So, excellent contact among the composite gradients resulted in raising the thermal conductivity values. Moreover, thermal conductivity of A359/5 wt.% AlN composite is 160.07 W/mK at a porosity percentage of 0.85% and that of A359/15 wt.% AlN composite is 163.30 W/mk at a relative porosity percentage of 1.85%. This signifies that increment in A359/AlN composite thermal conductivity is sensitive to the porosity percent. Otherwise, the thermal conductivity of A359/SiC composites substantially decreases as SiC amounts decrease. This is due to the relatively low thermal conductivity of SiC particulates, 77 W/mK, versus AlN, 190 W/mK, or even to A359 alloy, 158.2 W/mK. Besides, the porosity percentage is varied from 0.47% to 1.51% for A359/5 wt.% SiC and A359/15 wt.% SiC, respectively. This result reveals that the thermal conductivity of A359 composites is highly depending on the reinforcement type and the porosity percentage of the composite. Mizuuchi et al. (Ref 24, 51) reported that the porosity percentage lower than 1% is very significant in fabricating high thermal conductive Al/AlN composites.

Considerable attempts have been established to evaluate the thermal conductivity for different materials including metal-matrix composites. Among these attempts, Maxwell and Eucken (Ref 52) proposed a simplified form as compared to Hasselman-Johnson equation (Ref 53) assuming a perfect bonding between the particulates and the matrix in the produced composite. In this work, the following Maxwell-Eucken equation 1 is used for theoretical evaluation of composites thermal conductivity.

$$\lambda c = \lambda m \times ((2(\lambda p/\lambda m - 1)Vp + \lambda p/\lambda m + 2)/((1 - \lambda p/\lambda m)Vp + \lambda p/\lambda m + 2)) \quad \text{(Eq 1)}$$

where λc is the thermal conductivity of the composite, λp the thermal conductivity of the particulates (in the present investigation, 190 W/mK for AlN and 77 W/mK for SiC), λm the thermal conductivity of A359 matrix alloy (161 W/mK for A359), Vp the particulate volume fraction.

As shown in Table 1, the experimental results are nearly close to the calculated values using Maxwell-Eucken equation. These results confirm the strong bonding between the ceramic particulates and the A359 matrix alloy especially in A359/AlN composites. Moreover, it emphasizes the existence of minor or negligible damages around the particulates. Hence, squeeze casting process is considered to be an effective technique. It enhances the thermal conductivity by decreasing the composite porosity. Chedru et al. (Ref 26) and Zhang et al. (Ref 27) had conducted similar investigations to indicate the thermal conductivity of Al/AlN particulate composites prepared by a metal infiltration technique. It has been noticed that the thermal conductivity acquired in the current work is 160-163.3 W/mK at a weight percentage of AlN between 5% and 15%, while it is 131 W/mK (by Chedru et al. Ref 26) at 42% AlN and 130 W/mK (by Zhang et al. (Ref 27)) at 50%, respectively. This big difference and the marvelous enhancement of our measured thermal conductivity by comparison with the other reported results refer to particulates grade, where there are various grades of commercial AlN powders and the thermal conductivity rely on AlN grades and its purity. Beside the grade, matrix alloy and reinforcement particulates (type and size) are essential factors should be regarded. This is due to the large particle size that would be effective in decreasing the interfacial thermal resistance between particulate and matrix (Ref 24). In this work, beside the high-grade AlN and SiC, relatively large-sized particulates (40-45 μm) were used. The particulate size not only affects thermal conductivities but also improves the wear resistance. The particulates with larger size (as in this study) will be longer bonded within the matrix as compared to the smaller particulate size that easily detaches. This is in agreement with previous studies where sample with finer particles has more weight loss, while the sample with the larger size has the most favorable wear resistance (Ref 54, 55).

3.2 Change of Wear Rate with Load

The influence of load on the wear rate of A359/AlN composites is shown in Fig. 4(a). As indicated, the effect of AlN on the wear rate depends on the applied load. The composites show extraordinary wear resistance as compared to A359 alloy. A359 matrix is the most material liable to maximum wear rate at all loads. The wear rate decreases with increasing AlN particulates. On the other side, the influence of load on A359/SiC composites wear rate is shown in Fig. 4(b). Also, the wear rate shows analogous behavior where it

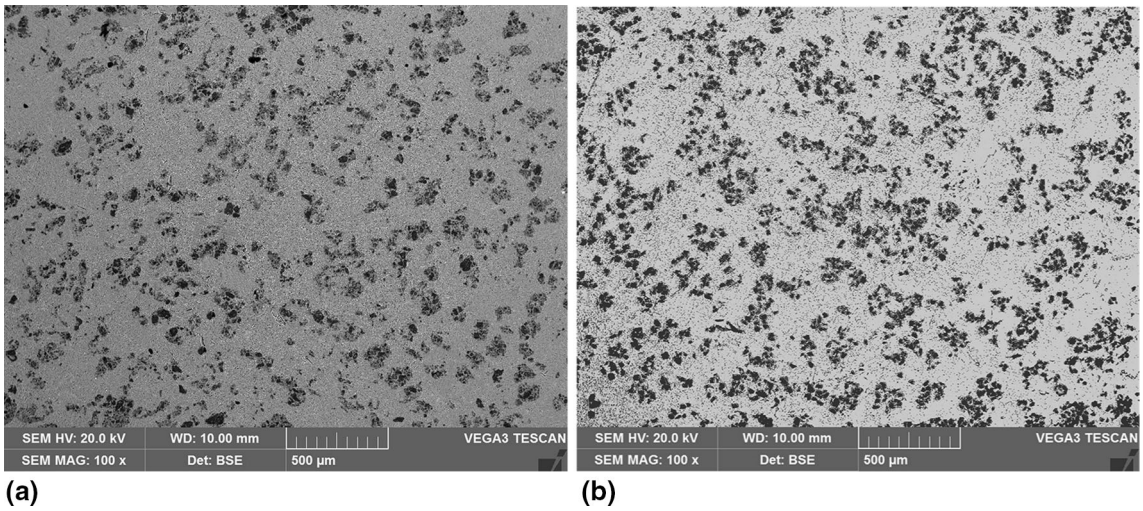

Fig. 1 Low magnification micrographs of squeeze cast: (a) A359/15% AlN, (b) A359/15% SiC

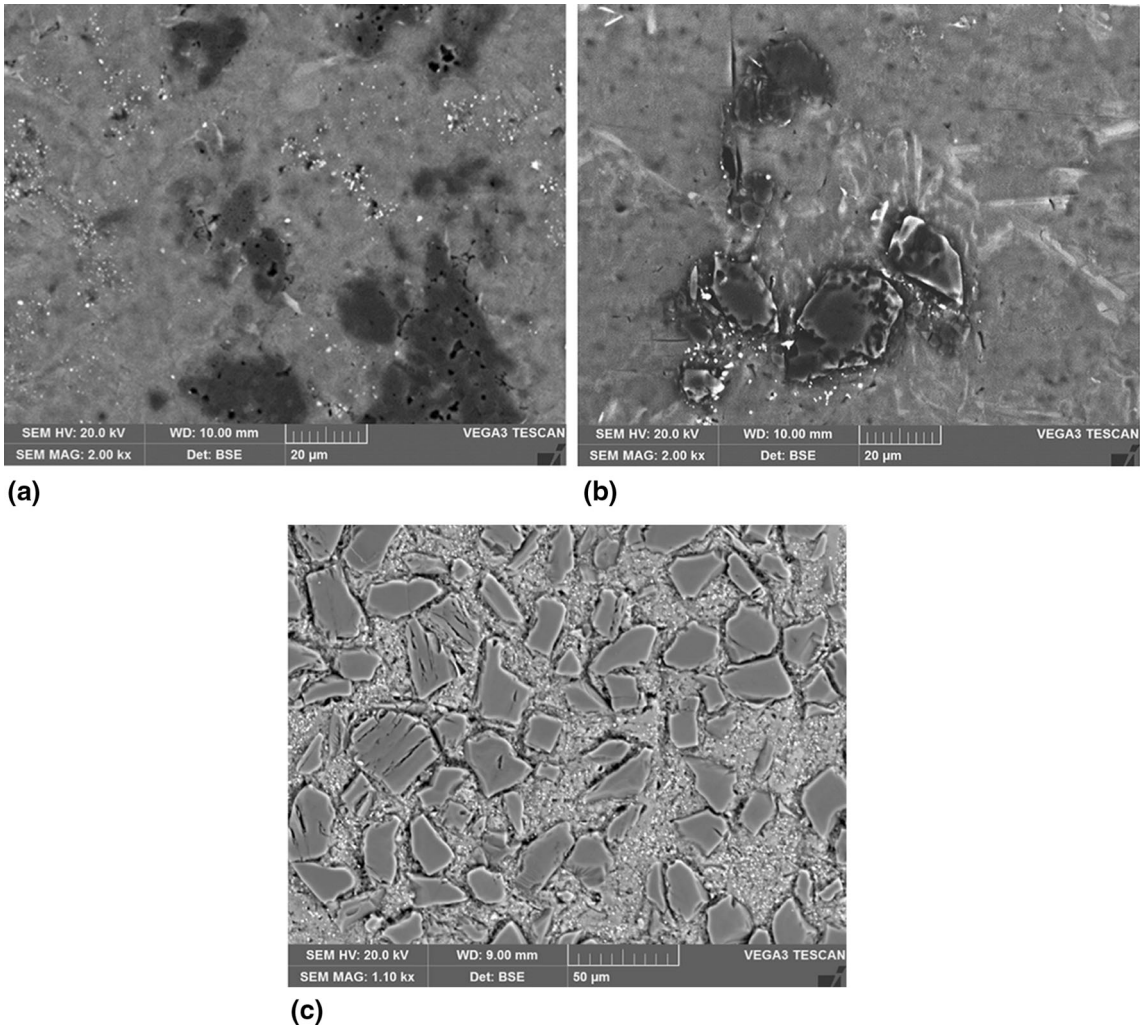

Fig. 2 SEM micrographs of squeeze cast: (a) A359/15% AlN, (b) A359/15% SiC, (c) A359/15% SiC

increases as load increases. In other words, A359/SiC composites exhibit a satisfactory increment in the wear resistance over A359 matrix alloy. However, A359/AlN composites reveal significant wear resistance versus A359 matrix or A359/SiC composites. As set out above, the higher thermal conductivity of A359/AlN composites plays an essential role in dissipation the frictional heat. At load of 20 N, the A359/AlN wear rate is nearly the same as that of A359/SiC composites. They have

much lower wear rates than that of the matrix alloy, while, at a load of 60 N, A359/AlN composites wear rate is lower and the difference between the wear rates of composites and A359 matrix is noticeable.

3.3 Influence of Load and Sliding Distance on the Friction Coefficient

Dependence of friction coefficient (μ) on load is illustrated in Fig. 5(a). Friction coefficients for all the tested materials slightly decrease with load at the load range of 20-60 N. Generally, friction coefficient values of A359/AlN composites are lower than that of A359 matrix alloy at the same load. This is due to the substantial effect of high thermal conductivity of AlN particulates which causes lower friction forces during the wear process.

Changes of friction coefficient with sliding distance at load of 60 N are presented in Fig. 5(b). Dependence of friction coefficients on sliding wear distance is shown in Fig. 5(b). Coefficient of friction values is increased during the sliding motion. A logical interpretation is that, while wear takes place, powder debris is built. This debris may be in contact with friction surfaces. Furthermore, the friction area between the two surfaces increases, resulting in an additional friction between wear debris and the contact surface. In addition, friction plastic deformation increases the amount of work hardening. As a result of elevated work hardening, the friction coefficient increases.

Moreover, AlN particulate may be broken, entrapped between the composite and counterface, and therefore results in increasing the friction coefficient as the sliding distance increases. Figure 5(c) shows the relation between load and the friction coefficient of A359/SiC composites. The same behavior in A359/AlN composites is observed. Friction coefficients of A359 composites increase with increasing load from 20 to 60 N. As expected and in contrast to the A359/AlN composites, A359/SiC composites friction coefficient exhibits an enhancement in wear resistance at all loads versus A359 matrix. This is resulting from the substantial hardness of SiC that induced high friction force during wear. Figure 5(d) shows the dependence of friction coefficients on the sliding distance at 60 N. Friction coefficient of A359/SiC composites increases, and its value becomes higher than A359 unreinforced matrix.

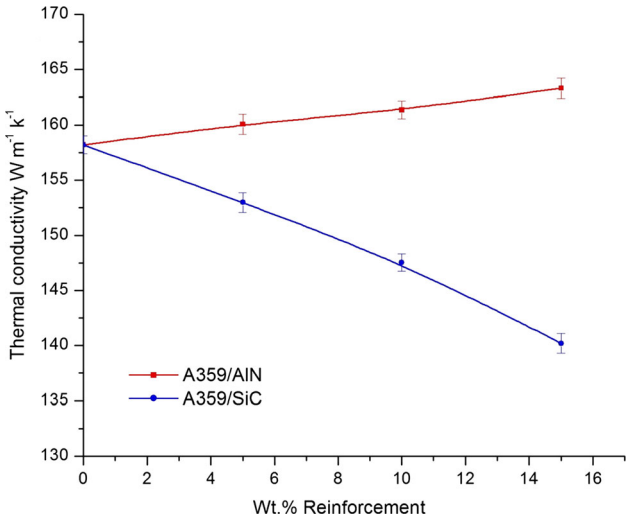

Fig. 3 Effect of reinforcement weight percentage on thermal conductivity

3.4 Changes of Composite Subsurface Temperature with Load

Heat generation and rising subsurface temperatures are mainly associated with friction. Most of the frictional energy is dissipated as heat (Ref 56). Figure 6(a) shows a variation of the subsurface temperature of A359/AlN composites with the applied load at different particle content. It is noted that the temperatures of the subsurface regions increased linearly with increasing the applied load. A359/AlN composites exhibit lower subsurface temperatures as compared to A359/SiC composites. This is attributed to the heat sink action of AlN particulates with high thermal conductivity. However, A359/SiC composites reveal high subsurface temperature as illustrated in Fig. 6(b). The higher addition of SiC particulates introduced, the more subsurface temperature evolved. Because of the increase in contact area and the existence of the wear debris between friction surfaces, the friction force increases, as a result, subsurface temperatures increase (Ref 57). The early work of Jaeger (Ref 58) has been reviewed in a simplified form by Bowden and Tabor (Ref 59). Basically, the temperature rise ($\Delta T = T - T_o$) is given as a function of the total heat developed:

$$\Delta T = \mu F g v / 4 J r (k1 + k2) \quad \text{(Eq 2)}$$

where T is steady-state temperature, To is the nominal temperature, μ is the sliding friction coefficient, F is the load, g is the acceleration due to gravity, v is the sliding velocity, r is radius of specimens, J is the mechanical equivalent of heat (4.186 J/cal) and $k1$, $k2$ = thermal conductivity of specimens and steel disk, respectively. Equation 2 is used to estimate the theoretical prediction of temperature rises during wear. The theoretical values are presented in Table 2.

This estimation is in good agreement with previous experimental measurements in another 2014 Al alloy reinforced with Al_2O_3 ceramic particles (Ref 60), where the difference between the nominal and the contact subsurface temperature was 19-30 °C.

A comparison between the experimental and theoretical data in Fig. 6 and Table 2 shows that the subsurface temperature rise is higher in the case of A359/SiC as compared to that in the A359/AlN. Hence, frictional heating induced in A359/AlN is lower than that in A359/SiC composites.

The frictional heating parameter (Ψ) can be calculated using the following relation (Ref 61):

Table 1 A comparison between the experimental and theoretical thermal conductivity of A359 composites

	A359	A359/5% AlN	A359/10% AlN	A359/15% AlN	A359/5% SiC	A359/10% SiC	A359/15% SiC
Theoretical	161.00	162.37	163.75	165.14	155.97	151.04	146.21
Experimental	158.20	160.07	161.35	163.30	152.97	147.54	140.21

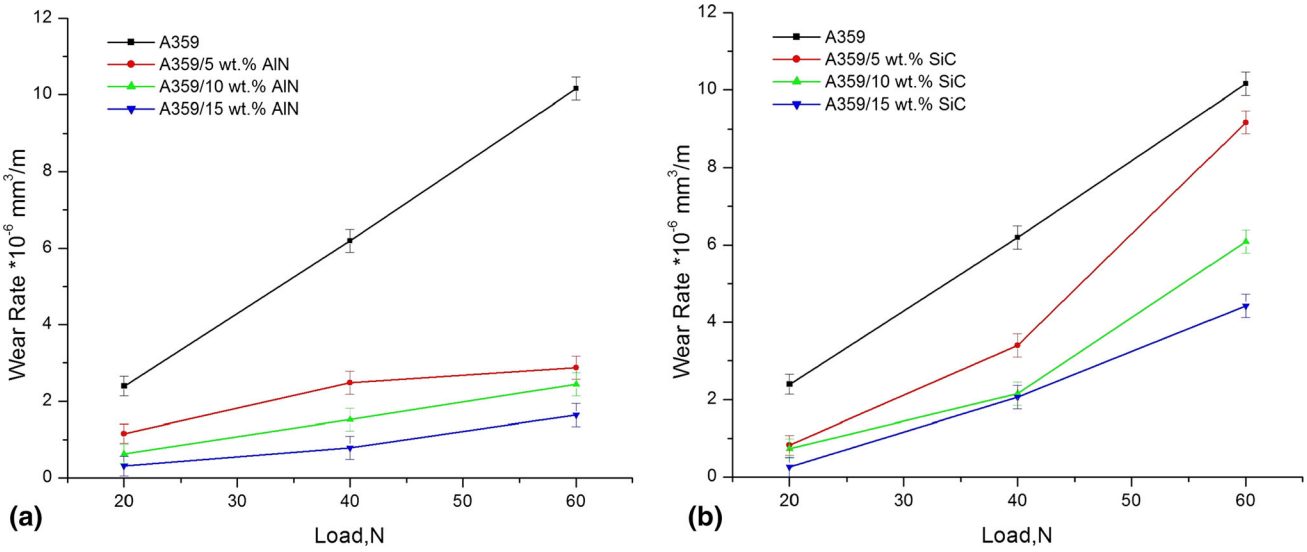

Fig. 4 Effect of load on wear rate: (a) A359/AlN, (b) A359/SiC

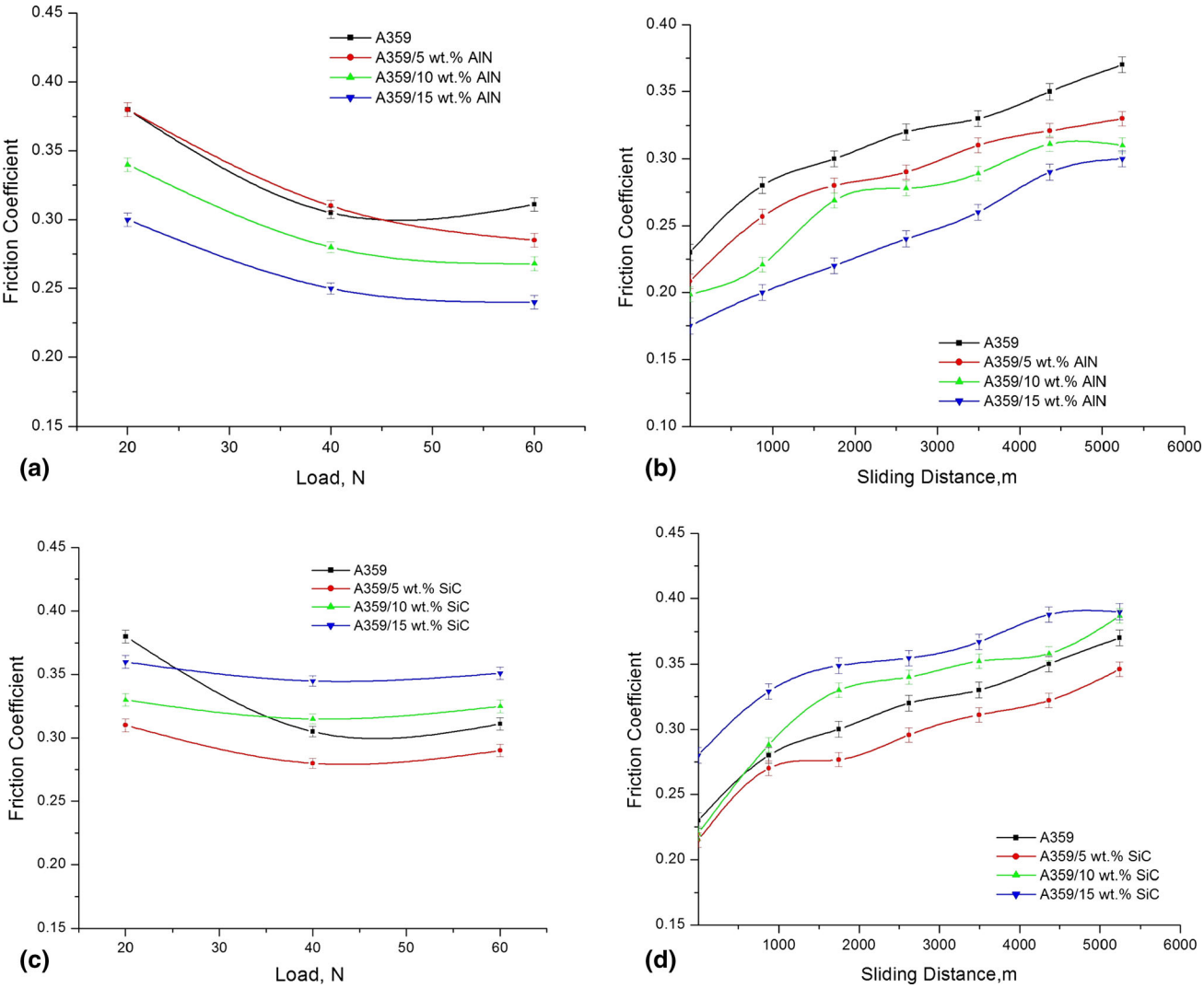

Fig. 5 Friction coefficient variation with load: (a) A359/AlN, (b) A359/SiC and sliding distance, (c) A359/AlN, (d) A359/SiC

$$\Psi = \Delta T / \mu F v t \quad \text{(Eq 3)}$$

where t is the sliding time (s). The frictional heating parameter for A359/15 wt.% AlN composite was found to be 2.4×10^{-4} °C/J, whereas it was 8.6×10^{-4} °C/J for A359/15 wt.% SiC under similar conditions. Blau et al. (Ref 61) have reported that the lower the frictional heating parameter, the less heat must be dissipated to the surroundings. Accordingly, it can be concluded that A359/15 wt.% AlN composite pins run much cooler than that of A359/15 wt.% SiC. The high thermal conductivity for AlN significantly decreases the Ψ value.

3.5 Worn Surface Morphology

SEM photographs of the A359 alloy at loads of 20 and 60 N are illustrated in Fig. 7(a) and (b). The existence of grooves, lips along wear direction pointed to vigorous plasticity particularly at 60 N. These photographs are used for comparison with other composites SEM photographs to study the influence of using different ceramic reinforcement particulates. These comparisons between worn surfaces will help to verify mechanisms of wear (Ref 62). Larger groove width at load of 60 N was observed as compared to that at load of 20 N.

On the other hand, the influences of using relatively high load on worn surfaces of A359 composites are illustrated in Fig. 8(a), (b), (c) and (d). The difference in the appearance of worn surfaces is clearly observed between the plastic deformation in higher and lower loads. As represented in Fig. 8(a) and (c), A359/AlN composites have a smooth worn surface free of large grooves or extensive lips that are clearly seen in A359/SiC composites regardless the reinforcement percentage as presented in Fig. 8(b) and (d). Here the superiority of AlN particulates over SiC is clearly revealed. A359/AlN composites show very high thermal conductivities with relatively low friction coefficients ranging from 0.268 to 0.295. Wear test is accompanied by plastic deformation at the pin surface. This plastic flow of metal at pin surface layer tends to mask AlN particulates and restrict their movement to the counterface until the metallic layer partially wore away. Then, friction force mills the AlN particulates into fine particulates and spreads them on the worn surface. Milled particulates are extended on the pin surface. They are sheared and joined to form a continuous film of solid AlN on the worn surface. During that, the solid AlN layer emerges from the broken AlN particulates and as wear proceeds, it propagates on composite pin surface. Then, AlN film is transferred to the counterface.

This process maintains an uninterrupted supply of AlN, which acts as a solid layer between two sliding surfaces. In short, the composite becomes more wear resistant due to transmission of broken AlN particulates to the tribosurfaces and their formation into a thin film. Therefore, the improvement in composite wear behavior depends on AlN ability to move out of their embedded positions in the matrix and evenly spread between tribological surfaces as a solid film (Ref 20, 57). Another important factor must be regarded is that AlN particulates with their exceptionally thermal conductivities act as a heat sink for the frictional heat induced during the wear process. Temperature of the pin specimen will quickly vanish. Thus, the mechanical properties of A359/AlN composite will keep away from any significant change.

A359/SiC composites worn surfaces as well as A359 matrix are characterized by harsh plastic deformation and damage as cavitation lips. This adhesive wear is pronounced as adhesive ploughing on the pin surface. A359 wear depends principally on cracks nucleation and propagation on tribological surfaces. In general, the available crack nucleation source in A359/SiC composites is the interface. In the initial period of wear process, SiC particulate resists the destructive effect and protects the surface. Then, cracks initiated and joined with each other to form wear debris. Additionally, the hard SiC particulates tend to fragment to minor pieces and separated out from the matrix. Fragmentation of particulate occurs when the applied stress is more than the fracture strength (Ref 62). The view of the extensive wear exhibited in Fig. 8(b) and (d) clearly reveals that a layer of material has been removed as debris from these areas. Also, A359/SiC composites worn surfaces are distinguished by numerous grooves; numerous short cracks more or less perpendicular to the sliding direction. These cracks probably have originated under pin wear surface and propagated to wear surface. This denotes the localized plastic deformation in the subsurface region adjacent to the contact surfaces. The deformation induced by shear results in generation of large strain in the pin layer. Localization of large strain in that layer results in crack initiation and propagation through the shear bands. Large plastic strains enhance voids nucleation

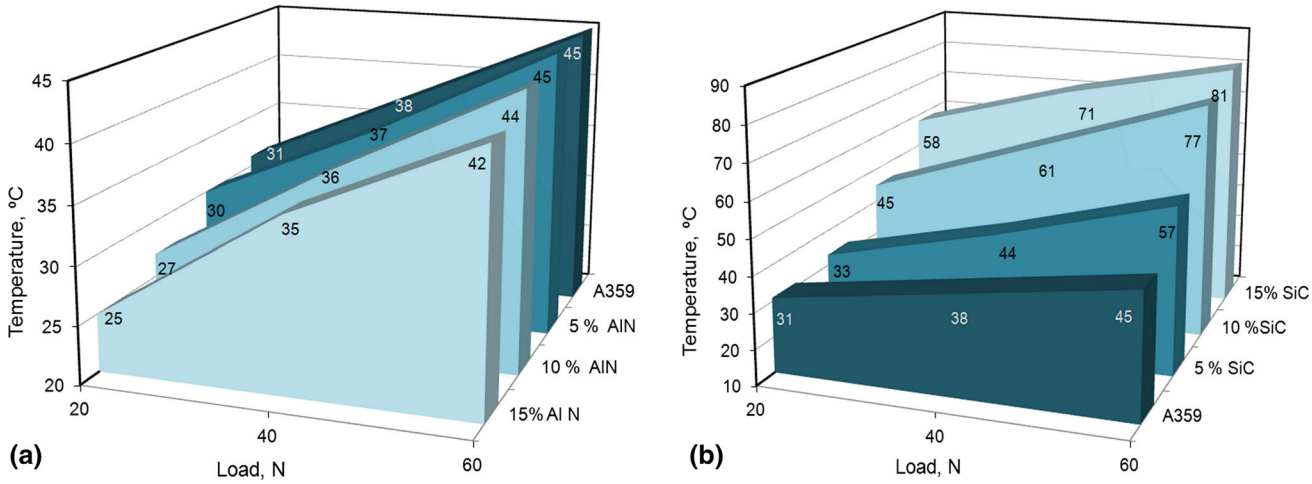

Fig. 6 Effect of load and reinforcement weight percentage on composite pin temperature: (a) A359/AlN, (b) A359/SiC

Table 2 Theoretical predictions of temperate rise at different loads

Load	A359	A359/5% AlN	A359/10% AlN	A359/15% AlN	A359/5% SiC	A359/10% SiC	A359/15% SiC
20	15.05	14.91	13.26	11.59	12.60	13.79	15.64
40	24.13	24.33	21.84	19.31	22.76	26.33	29.98
60	36.95	33.55	31.35	27.81	35.36	40.75	45.75

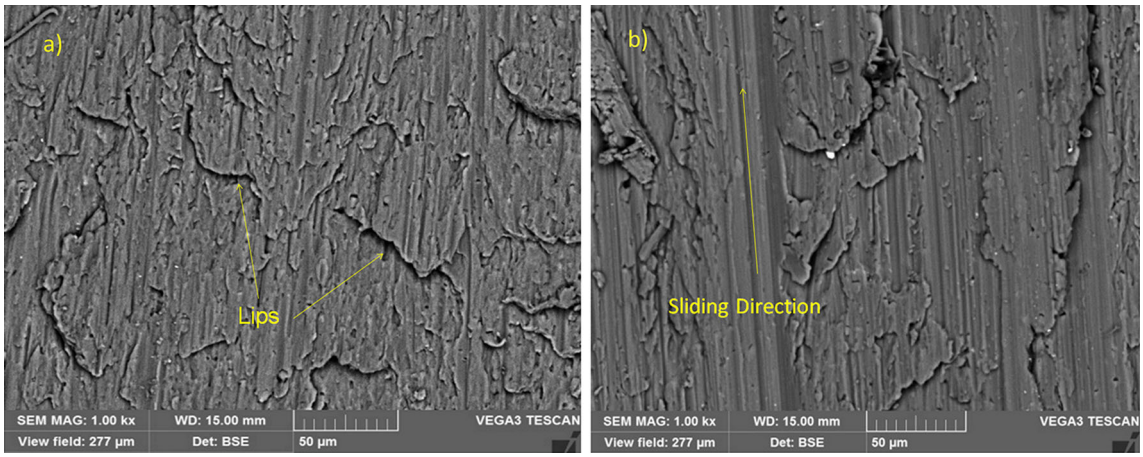

Fig. 7 SEM micrographs of the worn surfaces of the A359 alloy: (a) at load 20 N, (b) at load 60 N

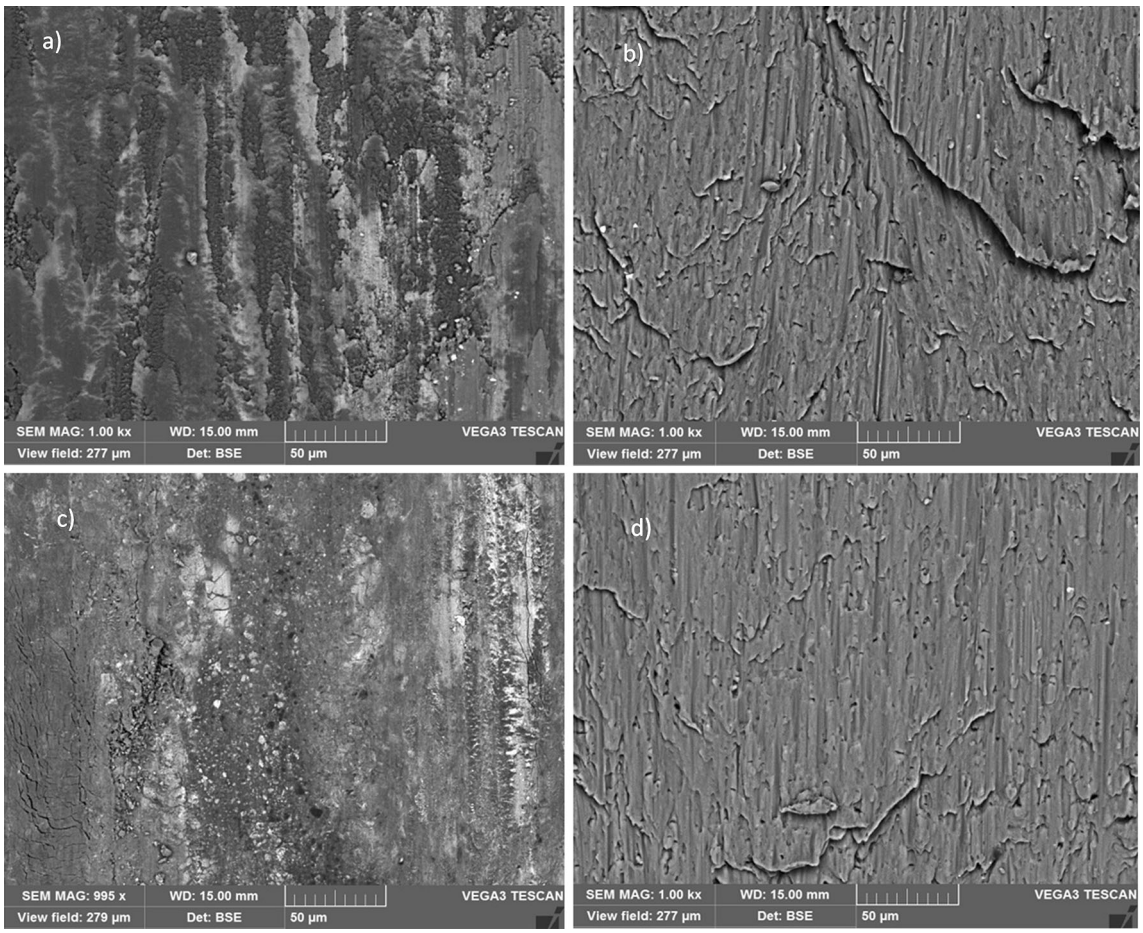

Fig. 8 SEM micrographs of the worn surfaces of the A359 composites at 60 N: (a) A359/5% AlN, (b) A359/5% SiC, (c) A359/15% AlN, (d) A359/15% SiC

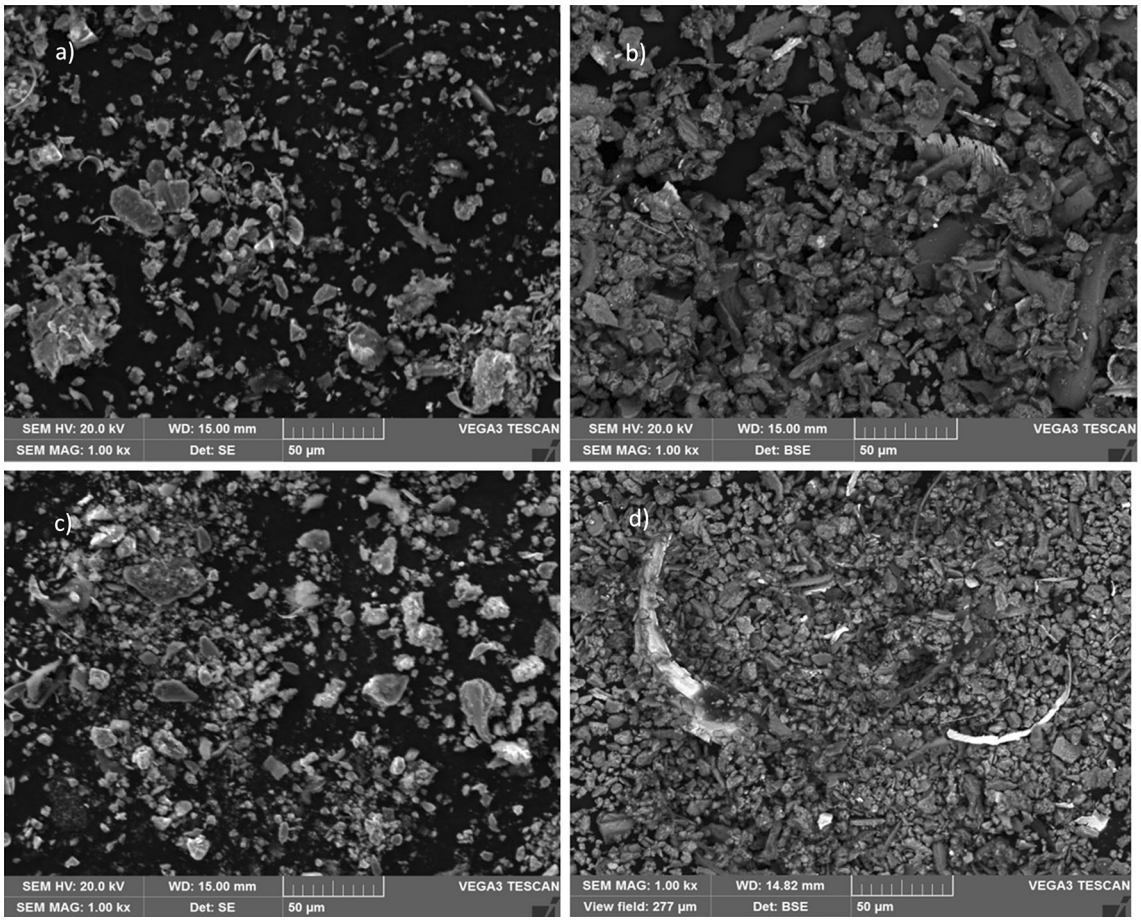

Fig. 9 SEM micrographs of the wear debris from the A359 composites at 60 N: (a) A359/5% AlN, (b) A359/5% SiC, (c) A359/15% AlN, (d) A359/15% SiC

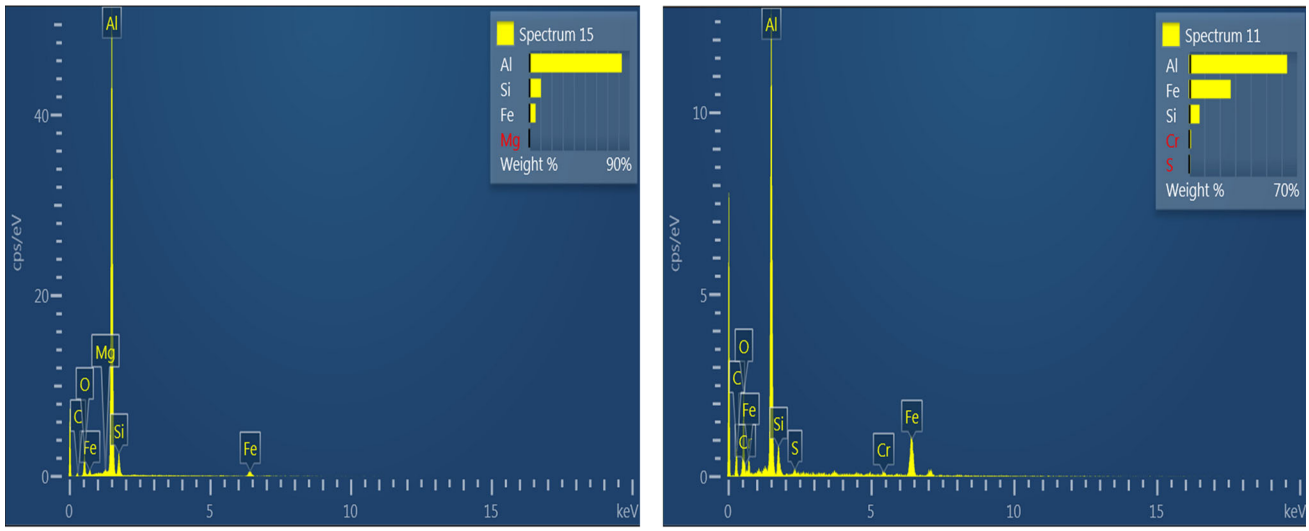

(a) **(b)**

Fig. 10 EDXA of the worn debris of the A359 composites tested at 60 N: (a) A359/15% AlN, (b) A359/15% SiC

and growth at the particulates located in subsurface regions. These voids are then coalescing to form cracks, allowing wear debris to delaminate (Ref 63).

Composites wear debris generated at load 60 N has forms of chips and fine particulates (Fig. 9). The amount of A359/SiC composite wear debris is relatively higher as compared to that

of A359/AlN composite (Fig. 9b and d). The smaller amount of the A359/AlN debris is related to the high thermal conductivity of AlN particulates. The composition of the debris was determined using EDXA investigation. The debris is observed to consist mainly of Al, Si, Mg, O and Fe (Fig. 10a and b). This result clearly pointed to the debris generated at high loads is a mechanical mixture of particulates detached from both the specimen and the counterface. Hence, the formation mechanisms of debris include surface delamination and abrasion. The presence of Fe in the debris is regarded as a sign of abrasion action of the exposed tips of AlN or SiC particulates on the steel counterface. The broken fragments of these ceramic particulates, which mixed with the loose debris, may act as a third abrasive material of both composite and steel.

4. Conclusions

In the present work, the following conclusions are deduced:

1. The microstructures of the squeeze cast composites show relatively uniform distribution of AlN and SiC particles within the A359 matrix alloy.
2. A359/AlN composites thermal conductivities are slightly increased as the weight percentage of AlN particulates in the A359 matrix alloy increased. However, it shows a significant decrease with increasing SiC content in A359/SiC composites.
3. A359 alloy reinforced with AlN or SiC exhibits a superior wear resistance as compared to A359 matrix alloy.
4. Wear rates of A359 reinforced with AlN or SiC particulates are decreased with the addition of particulates.
5. A359/AlN composites exhibit excellent wear resistance than that of A359/SiC composites at relatively high loads.
6. Contact subsurface temperatures increased as the load increased for all tested materials. It increased in A359/SiC composites with boosting SiC content. However, it slightly decreased as wt% AlN increased.
7. Friction coefficients of A359/SiC composites are higher than that of A359 alloy. On the other hand, friction coefficients of A359/AlN composites are lower.
8. A359/AlN composites worn surfaces were covered by aluminum nitrides and iron oxides, which acted as a smooth soft layer. However, A359/SiC composites were only smeared by iron oxides.

Acknowledgments

The authors express gratitude to Russian Federation Ministry of Education and Science for financial aid in the framework of Increase Competitiveness Program of NUST "MISiS" (No K1-2014-026 and K2-2015-073).

References

1. H. Kala, K.K.S. Mer, and S. Kumar, A Review on Mechanical and Tribological Behaviors of Stir Cast Aluminum Matrix Composites, *Procedia Materials Science*, 2014, **6**, p 1951–1960
2. M.J. Ghazali, W.M. Rainforth, and H. Jones, The Wear of Wrought Aluminium Alloys Under Dry Sliding Conditions, *Tribol. Int.*, 2007, **40**, p 160–169
3. S. Suresh, N.S.V. Moorthi, S.C. Vanettivel, N. Selvakumar, and G.R. Jinu, Effect of Graphite Addition on Mechanical Behavior of Al6061/TiB_2 Hybrid Composite Using Acoustic Emission, *Mater. Sci. Eng. A*, 2014, **612**, p 16–27
4. G.S. Wang and L. Geng, Microstructural Changes of SiCw/6061Al Composite During Compression at Temperatures Below and Above the Solidus of the Matrix Alloy, *Mater. Chem. Phys.*, 2006, **96**, p 2–8
5. N.M. Kumar, S.S. Kumaran, and L.A. Kumaraswamidhas, High Temperature Investigation on EDM Process of Al 2618 Alloy Reinforced with Si_3N_4, ALN and ZrB_2 In Situ Composites, *J. Alloy. Compd.*, 2016, **663**, p 755–768
6. M. Kok, Abrasive Wear of Al_2O_3 Particle Reinforced 2024 Aluminium Alloy Composites Fabricated by Vortex Method, *Compos. A*, 2006, **37**, p 457–464
7. B.N. Sarada, P.L. Srinivasa Murthy, and G. Ugrasen, Hardness and wear characteristics of Hybrid Aluminium Metal Matrix Composites produced by stir casting technique, Materials Today: Proceedings, 2015, (2), p 2878–2885
8. Y. Liu, Z. Han, and H. Cong, Effects of Sliding Velocity and Normal Load on the Tribological Behavior of a Nanocrystalline Al Based Composite, *Wear*, 2010, **268**, p 976–983
9. S. Suresh, N.S.V. Moorthi, N. Vettivel, and S.C. Selvakumarn, Mechanical Behavior and Wear Prediction of Stir Cast Al–TiB_2 composites Using Response Surface Methodology, *Mater. Des.*, 2014, **59**, p 383–396
10. J. Liu, J. Binner, and R. Higginson, Dry Sliding Wear Behaviour of Co-Continuous Ceramic Foam/Aluminium Alloy Interpenetrating Composites Produced by Pressureless Infiltration, *Wear*, 2012, **276–277**, p 94–104
11. S.K. Chaudhury, A.K. Singh, C.S. Sivaramakrishnan, and S.C. Panigrahi, Wear and Friction Behavior of Spray Formed and Stir Cast Al–2 Mg–11TiO_2 Composites, *Wear*, 2005, **258**, p 759–767
12. Y. Wang, W.M. Rainforth, H. Jones, and M. Lieblich, Dry Wear Behaviour and Its Relation to Microstructure of Novel 6092 Aluminium Alloy–Ni_3Al Powder Metallurgy Composite, *Wear*, 2001, **251**, p 1421–1432
13. J.C. Walker, W.M. Rainforth, and H. Jones, Lubricated Sliding Wear Behaviour of Aluminium Alloy Composites, *Wear*, 2005, **259**, p 577–589
14. A. Daoud, Wear Performance of 2014 Al Alloy Reinforced with Continuous Carbon Fibers Manufactured by Gas Pressure Infiltration, *Mater. Lett.*, 2004, **58**, p 3013–3206
15. A. Lekatou, A.E. Karantzalis, A. Evangelou, V. Gousia, G. Kaptay, Z. Gácsi, P. Baumli, and A. Simon, Aluminium Reinforced by WC and TiC Nanoparticles (ex situ) and Aluminide Particles (in situ): Microstructure, Wear and Corrosion Behavior, *Mater. Des.*, 2015, **65**, p 1121–1135
16. A. Mazahery and M.O. Shabani, Influence of the Hard Coated B_4C Particulates on Wear Resistance of Al–Cu Alloys, *Compos. B*, 2012, **43**, p 1302–1308
17. P. Ravindran, K. Manisekar, R. Narayanasamy, and P. Narayanasamy, Tribological Behavior of Powder Metallurgy-Processed Aluminium Hybrid Composites with the Addition of Graphite Solid Lubricant, *Ceram. Int.*, 2013, **39**, p 1169–1182
18. M.V. Gorshenkov, S.D. Kaloshkin, V.V. Tcherdyntsev, V.D. Danilov, and V.N. Gulbin, Dry Sliding Friction of Al-Based Composites Reinforced with Various Boron-Containing Particles, *J. Alloy. Compd.*, 2012, **536**, p S126–S129
19. A. Daoud and M.T. AbouEl-khair, Wear and Friction Behavior of Sand Cast Brake Rotor made of A359-20 vol.% SiC Particle Composites Sliding Against Automobile Friction Material, *Tribol. Int.*, 2010, **43**, p 544–553
20. A. Daoud, M.T. Abou El-khair, and P. Rohatgi, Wear and friction behavior of near eutectic Al-Si + ZrO_2 or WC Particle Composites, *Compos. Sci. Technol.*, 2004, **64**, p 1029–1040
21. J. Wang, D. Yi, X. Su, F. Yin, and H. Li, Properties of Submicron AlN Particulate Reinforced Aluminum Matrix Composite, *Mater. Des.*, 2009, **30**, p 78–81
22. L. Jia, K. Kondoh, H. Imai, M. Onishi, B. Chen, and S. Li, Nano-Scale AlN Powders and AlN/Al Composites by Full and Partial Direct

Nitridation of Aluminum in Solid-State, *J. Alloy. Compd.*, 2015, **629**, p 184–187
23. B.A. Kumar, N. Murugan, and I. Dinaharan, Dry Sliding Wear Behavior of Stir Cast AA6061-T6/AlNp Composite, *Trans. Nonferrous Met. Soc. China*, 2014, **24**, p 2785–2795
24. K. Mizuuchi, K. Inoue, Y. Agari, T. Nagaoka, M. Sugioka, M. Tanaka, T. Takeuchi, J. Tani, M. Kawahara, Y. Makino, and M. Ito, Processing and Thermal Properties of Al/AlN Composites in Continuous solid–liquid co-Existent State by Spark Plasma Sintering, *Compos. B*, 2012, **43**, p 1557–1563
25. A. Kalemats, G. Topates, O. Bahadir, P.K. Isci, and H. Mandal, Thermal Properties of Pressureless Melt Infiltrated AlN-Si-Al Composites, *Trans. Nonferrous Met. Soc. China*, 2013, **23**, p 1304–1313
26. M. Chedru, J.L. Chermant, and J. Vicens, Thermal Properties and Young's Modulus of Al-AlN Composites, *J. Mater. Sci. Lett.*, 2001, **20**, p 893–895
27. Q. Zhang, G. Chen, G. Wu, Z. Xiu, and B. Luan, Property Characteristics of a AlNp/Al Composite Fabricated by Squeeze Casting Technology, *Mater. Lett.*, 2003, **57**, p 1453–1458
28. I.L. Tangen, Y. Yu, T. Grande, T. Mokkelbost, R. Høier, and M.A. Einarsrud, Preparation and Characterisation of Aluminium Nitride–Silicon Carbide Composites, *Ceram. Int.*, 2004, **30**, p 931–938
29. B.N. Pramila Bai, B.S. Ramasesh, and M.K. Surappa, Dry Sliding Wear of A356-Al-SiCp Composites, *Wear*, 1992, **157**, p 295–304
30. S.K. Sharma, B.V.M. Kumar, K.Y. Lim, Y.W. Kim, and S.K. Nath, Erosion Behavior of SiC-WC Composites, *Ceram. Int.*, 2014, **40**, p 6829–6839
31. Z. Wang, X. Wang, Y. Zhao, and W. Du, SiC Nanoparticles Reinforced Magnesium Matrix Composites Fabricated by Ultrasonic Method, *Trans. Nonferrous Met. Soc. China*, 2010, **20**, p 1029–1032
32. A. Shaga, P. Shen, Ch Sun, and Q. Jiang, Lamellar-Interpenetrated Al-Si-Mg/SiC Composites Fabricated by Freeze Casting and Pressureless Infiltration, *Mater. Sci. Eng. A*, 2015, **630**, p 78–84
33. L. Micele, G. Palombarini, S. Guicciardi, and L. Silvestroni, Tribological Behaviour and Wear Resistance of a SiC-$MoSi_2$ composite Dry Sliding Against Al_2O_3, *Wear*, 2010, **269**, p 368–375
34. E.A. Shalaby, A.Y. Churyumov, A.N. Solonin, and A. Lotfy, Preparation and Characterization of Hybrid A359/(SiC + Si_3N_4) Composites Synthesized by Stir/Squeeze Casting Techniques, *Mater. Sci. Eng. A*, 2016, **674**, p 18–24
35. D. Przestacki, P. Szymanski, and S. Wojciechowski, Formation of Surface Layer in Metal Matrix Composite A359/20SiC_P During Laser Assisted Turning, *Compos. A*, 2016, **91**, p 370–379
36. P.K. Rohatgi, R.B. Thakkar, J.K. Kim, and A. Daoud, Scatter and Statistical Analysis of Tensile Properties of cast SiC reinforced A359 alloys, *Mater. Sci. Eng. A*, 2005, **398**, p 1–14
37. A. Madgwick, C. Ungpinitpong, T. Mori, and P.J. Withers, Observation and Quantitative Analysis of Damage Caused by Creep in an A1A359/SiC_P Composite, *Mater. Sci. Eng. A*, 2003, **342**, p 201–206
38. R. Rodríguez-Castro, R.C. Wetherhold, and M.H. Kelestemur, Microstructure and Mechanical Behavior of Functionally Graded AlA359/SiCp Ccomposite, *Mater. Sci. Eng. A*, 2002, **323**, p 445–456
39. P.K. Rohatgi, S. Alaraj, R.B. Thakkar, and A. Daoud, Variation in Fatigue Properties of cast A359-SiC Composites Under Total Strain Controlled Conditions: Effects of Porosity and Inclusions, *Compos. A*, 2007, **38**, p 1829–1841
40. Y. Li, K.T. Ramesh, and E.S.C. Chin, Comparison of the Plastic Deformation and Failure of A359/SiC and 6061-T6/Al_2O_3 metal Matrix Composites Under Dynamic Tension, *Mater. Sci. Eng. A*, 2004, **371**, p 359–370
41. Y. Li, K.T. Ramesh, and E.S.C. Chin, The mechanical Response of an A359/SiC_p MMC and the A359 Aluminum Matrix to Dynamic Shearing Deformations, *Mater. Sci. Eng. A*, 2004, **382**, p 162–170
42. M. Gajewska, J. Dutkiewicz, and J. Morgiel, Microstructure and Mechanical Properties of AA7475/AlN Compacts with Varied Reinforcing Particles Size, *Compos. Theory Pract.*, 2012, **12**, p 177–181
43. J.B. Fogagnolo, M.H. Robert, and J.M. Torralba, Mechanically Alloyed AlN Particle-Reinforced Al-6061 Matrix Composites: Powder Processing, Consolidation and Mechanical Strength and Hardness of the As-Extruded Materials, *Mater. Sci. Eng. A*, 2006, **426**, p 85–94
44. M. Gajewska, J. Dutkiewicz, and J. Morgiel, Effect of Reinforcement Particle Size on Microstructure and Mechanical Properties of Al Zn Mg Cu/AlN Nano-Composites Produced Using Mechanical Alloying, *J. Alloy. Compd.*, 2014, **586**, p S423–S427
45. H.B. Michael Rajan, S. Ramabalan, I. Dinaharan, and S.J. Vijay, Synthesis and Characterization of In Situ Formed Titanium Diboride Particulate Reinforced AA7075 Aluminum Alloy Cast Composites, *Mater. Des.*, 2013, **44**, p 438–445
46. J.W. Kaczmar, K. Pietrzak, and W. Wlosinski, The Production and Application of Metal Matrix Composite Materials, *J. Mater. Process. Technol.*, 2000, **106**, p 58–67
47. M.M. Schwartz, *Composite Materials Volume II: Processing, Fabrication, and Applications*, ASM International, 1997
48. M.T. Abou El-Khair, A. Daoud, and A.N. Abdel Azim, Effect of Casting Technology on the Wear Behaviour of A356 Al-Al_2O_3 or ZrO_2 Composites. 4th Arab Cast Conference, 2002
49. A. Daoud, M.T. Abou El-Khair, and A.N. Abdel Azim, Microstructure and Wear Behavior of Squeeze Cast 7075 A-Al_2O_3 Particle Composites. 14th International Offshore and Polar Engineering Conference, 2004
50. M. Kamara and A. Ramesh, Effect of Squeeze Pressure on Mechanical Properties of LM6 Aluminium Alloy Matrix Hybrid Composite, *ARPN J. Eng. Appl. Sci.*, 2015, **10**, p 6051–6058
51. K. Mizuuchi, K. Inoue, Y. Agari, Y. Morisada, M. Sugioka, M. Tanaka, T. Takeuchi, J. Tani, M. Kawahara, Y. Makino, and M. Ito, Thermal Properties of Diamond Particle Dispersed Aluminum Matrix Composites Fabricated in Continuous Solid–Liquid Co-Existent State by SPS, *J. Jpn. Soc. Powder Metall.*, 2009, **56**, p 438–443
52. A. Eucken, Heat transfer in ceramic refractory materials: calculation from thermal conductivities of constituents, Fortchg. Gebiete Ingenieurw., B.3. Forschungsheft. 1932, (16), p 353–360
53. D.P.H. Hasselman and F.J. Lloyd, Effective Thermal Conductivity of Composites with Interfacial Thermal Barrier Resistance, *J. Compos. Mater.*, 1987, **21**, p 508–515
54. A.A. Cerit, M.B. Karamis, F. Nair, and K. Yildizli, Effect of Reinforcement Particle Size and Volume Fraction on Wear Behaviour of Metal Matrix Composites, *Tribol. Ind.*, 2008, **30**, p 31–36
55. P.S. Sahu and R. Banchhor, Effect of Silicon Carbide Reinforcement on Wear and Tribological Properties of Aluminium Matrix Composites, *Int. J. Innov. Sci. Eng. Technol.*, 2016, **3**, p 293–299
56. J. Paulo Davim, *Tribology in Manufacturing Technology*, London, 2012, p 90–93
57. T. Maiyajima and Y. Iwai, Effects of Reinforcements on Sliding Wear Behavior of Aluminum Matrix Composites, *Wear*, 2003, **255**, p 606–616
58. J.C. Jaeger, Moving Sources of Heat and the Temperature at Sliding Contacts, *J. Proc. R. Soc. N. South Wales*, 1942, **76**, p 203–224
59. F.P. Bowden and D. Tabor, *The Friction and Lubrication of Solids*, Clarendon Press, Oxford, 1986
60. J. Rodriaguez, A. Martin, and J. Llorca, Modling the Effect of Temperature on the Wear Resistance of Metals Reinforced with Ceramic Particles, *Acta Mater.*, 2000, **48**, p 993–1003
61. P.J. Blau, B.C. Jolly, J. Qu, W.H. Peter, and C.A. Blue, Tribological Investigation of Titanium-Based Materials for Brakes, *Wear*, 2007, **263**, p 1202–1211
62. H. Zhang, M.W. Chen, K.T. Ramesh, J. Ye, J.M. Schoenung, and E.S.C. Chin, Tensile Behavior and Dynamic Failure of Aluminum 6092/B_4C Composites, *Mater. Sci. Eng. A*, 2006, **433**, p 70–82
63. P. Cavaliere, E. Cerri, and P. Leo, Effect of Heat Treatments on Mechanical Properties and Damage Evolution of Thixoformed Aluminium Alloys, *Mater. Charact.*, 2005, **55**, p 35–42